Heliyon 10 (2024) e24460

Contents lists available at ScienceDirect

Heliyon

journal homepage: www.cell.com/heliyon

Research article

Human serum albumin-bound paclitaxel nanoparticle inhibits cervical carcinoma cell proliferation and oxidative damage through CYP3A4 and CYP2C8

Haojue Wang [a,d,1], Dajun Xiang [a,1], Xianyi Lu [a], Ling Fang [b], Chengjun Cui [c], Qifeng Shi [c], Xiaojun Yang [d,*]

[a] Department of Obstetrics and Gynecology, Wuxi Xishan People's Hospital, (Wuxi Branch of Zhongda Hospital Southeast University), 214015, Wuxi, Jiangsu, China
[b] Department of Dermatology, Wuxi Xishan People's Hospital, (Wuxi Branch of Zhongda Hospital Southeast University), Wuxi, Jiangsu, 214105, China
[c] Department of Pathology, Wuxi Xishan People's Hospital, (Wuxi Branch of Zhongda Hospital Southeast University), Wuxi, Jiangsu, 214105, China
[d] The First Affiliated Hospital of Soochow University, Suzhou, Jiangsu, 215006, China

ARTICLE INFO

Keywords:
Human serum albumin
Paclitaxel
Cervical carcinoma
CYP3A4
CYP2C8
Oxidative damage

ABSTRACT

Background: Cervical cancer (CC) is currently the most common malignant tumour in the female reproductive tract, and paclitaxel (PTX) is a commonly used chemotherapeutic agent, but tumour cell resistance will seriously affect the therapeutic efficacy of PTX. Nanoparticle human serum albumin-bound paclitaxel (Nano-HSA-PTX) is a novel drug delivery modality that may have superior effects to PTX alone.

Objective: To clarify the effect of Nano-HSA-PTX on cervical carcinoma (CC) cells and the underlying mechanisms.

Methods: After the preparation of Nano-HSA-PTX, its morphology was observed by electron transmission microscope (TEM), and its entrapment efficiency (EE%) and drug loading rate (DL%) were detected. Nano-HSA-PTX was compared with conventional PTX for drug metabolism. Additionally, CC HeLa and SiHa cells were purchased and divided into three groups to treat with Nano-HSA-PTX, PTX and normal saline, respectively. MTT, cell cloning, Transwell and cell scratch assays were carried out to determine cell proliferation, invasion and migration, flow cytometry and Western blotting were performed to detect apoptosis rate and apoptosis-related protein expression, and PCR was conducted to quantify oxidative damage indicators. Further, CYP3A4 and CYP2C8 expression patterns in CC cells (HeLa and SiHa) and human normal cervical epithelia (End1/E6E7) and the changes of their levels under the intervention of Nano-HSA-PTX were measured. Subsequently, C57BL/6mice were purchased for subcutaneous tumorigenesis experiment to observe the impact of Nano-HSA-PTX on tumor growth.

Results: Under TEM, Nano-HSA-PTX was complete and arranged compactly, with a stable structure and markedly higher EE% and DL% than PTX ($P < 0.05$). Under Nano-HSA-PTX intervention, the proliferation, invasion, migration and oxidative damage of HeLa and SiHa were significantly decreased compared with the control and PTX groups, while the apoptosis was increased ($P < 0.05$). Besides, elevated CYP3A4 and CYP2C8 levels were observed in CC cells, which were

* Corresponding author.
E-mail address: xjyang@suda.edu.cn (X. Yang).
[1] These authors contributed equally to this work.

https://doi.org/10.1016/j.heliyon.2024.e24460
Received 17 October 2023; Received in revised form 28 December 2023; Accepted 9 January 2024
Available online 11 January 2024

inhibited by Nano-HSA-PTX and PTX ($P < 0.05$). Finally, tumorigenesis experiments in nude mice revealed that Nano-HSA-PTX could inhibit tumor growth.
Conclusion: Compared with PTX, Nano-HSA-PTX has a superior effect of inhibiting CC activity. And this mechanism of action was carried out by inhibiting the expression of CYP3A4 and CYP2C8.

1. Introduction

Despite the availability of relatively sound preventive vaccines, cervical carcinoma (CC) is currently the most common malignant mesonephric tumor with a high prevalence [1]. According to the World Health Organization (WTO) statistics 2018, the global incidence of CC is about 13/100,000, of which more than half of patients eventually die from it, this is due to the fact that CC tumour lesions can cause severe inflammatory damage and oxidative stress damage, which disrupts the normal functioning of the body's cells, tissues, and organs, ultimately leading to the patient's death due to organ failure [2]. In 2018, the cumulative surge of CC patients worldwide exceeded 560,000, with approximately 310,000 deaths [3]. Although there is a high cure rate for early-stage CC clinically, the prognosis of advanced CC leaves much to be desired [4]. Therefore, improving the early diagnosis of CC or cure rate of advanced CC has become a focus and difficulty in clinical research.

As nanotechnology continuously advances in recent years, nanomedicine is considered to be a new breakthrough in future cancer treatment [5]. Among them, using nanoparticles (NPs) as drug carriers can not only effectively improve drug targeting, reduce toxicities, but also enhance drug permeability into tissues [6,7]. At present, drug-loaded NPs are more and more extensively used in the medical field, in virtue of their advantages such as controllable particle size, high biocompatibility, easy phagocytosis by cells, and low drug selectivity [8]. As pointed out in the research, antibiotic-loaded NPs are an excellent treatment option for osteomyelitis [9]. Currently, drug delivery system based on nanoparticle human serum albumin-bound paclitaxel (Nano-HSA-PTX) was effective in the treatment of patients with recurrent CC, with excellent results achieved [10]. However, previous studies still present many limitations, such as limited research subjects included, single outcome measure that was only focused on patient survival, and little investigation regarding the specific influence mechanism of Nano-HSA-PTX on CC.

CYP3A4 and CYP2C8 are members of the cytochrome (CYP) family, which are closely related to a variety of malignancies including CC [11]. And in studies related to PTX, researchers have found that PTX can regulate apoptosis in breast and liver cancer cells through CYP3A4 and CYP2C8, and has the effect of regulating PTX-induced hepatotoxicity [12–14]. These studies have amply demonstrated that the killing mechanism of PTX on tumour cells is related to CYP3A4 and CYP2C8. Similarly, Nano-HSA-PTX may also be confirmed to affect tumour growth through these pathways, but studies on Nano-HSA-PTX are still relatively rare, and therefore we are unable to determine the relationship between Nano-HSA-PTX and CYP3A4, CYP2C8.

Currently, the morbidity and mortality of CC are increasing, and a full understanding of the effects of Nano-HSA-PTX on CC will probably provide new ideas for the future treatment of CC. Therefore, the present study will confirm the effect of Nano-HSA-PTX on CC by in vitro experiments and verify whether its mechanism of action is related to CYP3A4, CYP2C8, which will provide new references for future clinical treatment of CC.

2. Materials and methods

2.1. Cell data

Human CC cells (HeLa), human cervical squamous cell carcinoma (SiHa), and human normal cervical epithelial cells (End1/E6E7), all ordered from ATCC, were immersed in a medium that was composed of 10 % FBS plus 90 % DMED (37 °C, 5%CO_2) and changed every other day, until cell passage when cells were 70–80 % confluent.

2.2. Animal data

Forty 20–25 g SPF BALB/c female mice, aged 6–8 weeks (Jiangsu Rec-Biotech, SYXK (Su) 2021-0062), were reared with 5 animals per cage under the conditions of 20–26 °C, 40–70 % humidity, 12 h:12 h day/night alternation, and free eating and drinking. This study will strictly follow the animal welfare guidelines of the World Organization for Animal Health (OIE) Terrestrial Animal Health Code, and this study was also approved by the Animal Ethics Committee of the Infectious Animal Laboratory, Jiangsu Institute of Schistosomiasis Control (lACUC-JIPD-2023112).

2.3. Preparation of nano-HSA-PTX

Nano-HSA-PTX was prepared with reference to the study of Gao et al. [15]. 20 mg of PTX and 9 mL of polyethylene glycol (PEG) were weighed and dissolved in ethanol. The mixture of PTX and PEG was evaporated under vacuum and subsequently added to the HSA solution, and the mixture was stirred in the dark for 24 h. Following 48 h of dialysis in deionized water, the mixed solution was centrifuged (5000 rpm/min, 10 min), and the resulting supernatant was gathered. Thereafter, 10 mg HSA was weighed for dissolution in 0.05 g/mol NaCl-added PBS. 1 mg of PTX was weighed to dissolve in 1 mL of absolute ethanol, and the solution was then added

dropwise to the HSA solution while stirring. This was followed by dialysis in deionized water for 48 h, and supernatant separation after 10 min of centrifugation (5000 rpm/min), to obtain Nano-HSA-PTX.

2.4. Characterization and observation

The particle size distribution and surface Zeta potential (ZP) of Nano-HSA-PTX were measured using a nano-laser particle size analyzer, and the morphological characteristics were observed with an electron transmission microscope (TEM). Additionally, 1 mL of Nano-HSA-PTX was incubated in 10 % FBS-added DMEM complete medium (37 °C) and PBS with pH 7.4 (4 °C) for 7 days, respectively. Changes in particle size distribution and surface ZP were measured every 24 h.

2.5. Encapsulation efficiency (EE%) and drug loading rate (DL%) detection

After ultrasonic mixing of 1 mL of Nano-HSA-PTX and 9 mL of acetonitrile, the mixture was centrifuged (1200 rpm/min, 15min) to obtain supernatant, for the determination of PTX content (A value) by high-performance liquid chromatography (HPLC). In addition, 1 mL of Nano-HSA-PTX was freeze-dried and the total mass (B value) was determined. Subsequently, EE% and DL% of Nano-HSA-PTX were calculated using the following formulas: EE% = A value/PTX dosage × 100 %; DL% = A value/B value × 100 %. The EE% and DL % of PTX (liposome for injection, Nanjing Luye Pharmaceutical Co., Ltd., H20030357) were also detected as described above.

2.6. In vitro release assay

Nano-HSA-PTX and PTX, 3 mL each, were placed into dialysis bags and then into a container containing 30 % release medium, for oscillation blending at 37 °C. Samples with a volume of 3 mL were collected every 2 h to measure PTX in the removed release medium by HPLC, and the cumulative drug release rate of Nano-HSA-PTX was calculated.

2.7. In vitro cytotoxicity observation

HeLa and SiHa were incubated overnight at 37 °C and 5%CO_2 after being planted into the wells of 96-well plates. Then, the culture solution of each well was replaced with Nano-HSA-PTX with the concentrations of 25, 50, 100 and 200 μg/mL, respectively, for 48 h of continuous culture. After the addition of 20 μL MTT solution into each well, the absorbance value was detected by microplate reader (490 nm), and the concentration with the most significant inhibition effect was used as the basis for subsequent study.

2.8. CC cell grouping and intervention

According to the above experimental results, CC cells were cultured in the medium containing Nano-HSA-PTX solution and PTX solution, respectively, another equal amount of cells cultured in normal medium was set up as the control group. Follow-up experiments were carried out 24 h after culture.

2.9. MTT assay detects cell proliferation

The three groups of cells were seeded in 96-well plates, and added with 5 mg/mL MTT solution at 20 μL/well after 24 h, 48 h and 72 h of culture, followed by cell absorbance determination and growth curve plotting using the method described above.

2.10. Cell cloning assay detects cell proliferation

We cultured cells for 14 days after planting them into the wells of a 12-well plate (300/well), and changed the medium every 3 days. Following 30 min of crystal violet (2 %) staining at 37 °C, the cells cloned were counted under a light microscope to calculate the clone rate.

2.11. Transwell detects cell invasion

After the above three groups of cells were starved for 12 h, DMSO was added to re-suspend the cells (the concentration of cell suspension was adjusted to 5×10^5/mL). Subsequently, the cell suspension was inoculated into the upper chamber of the Transwell, and the DMSO medium was inoculated into the lower chamber of the Transwell, and incubated in a constant temperature incubator for 24 h (37 °C, 5CO_2).

2.12. Cell scratch test detects cell migration

The transmembrane cells were immobilized with formaldehyde, stained with 4 % crystal violet solution, and counted in 5 fields randomly selected under a microscope (200 ×). Another three groups of cells were set up, which were treated with a 10 μL sampling pipette tip for straight scratches when the fusion degree was close to 100 %. Twenty-four hours later, the scratch healing was observed under a 40-fold microscope, and photos were taken for preservation. Image J calculated the migration area of cells on the scratch and

the scratch healing rate.

2.13. Flow cytometry detects cells apoptosis

The three groups of cell suspensions were added to 6-well culture plates for 24 h and then the supernatant was separate. After rinsing with precooled PBS 3 times, they were re-suspended in 100 μL binding buffer, and added with AnnexinV and PI in turn (5 μL each), for 15 min of dark incubation. Flow cytometry determined the apoptosis rate. In addition, apoptosis-related proteins Bax and Bcl-2 were detected by Western blotting (WB). Cells were lysed by adding RIPA buffer and separated by SDS-PAGE, and after PVDF membrane transfer, they were sealed with 5 % skim milk for 2 h and washed before incubation (4 °C) with primary antibodies overnight. After washing the second day, it was added with a second antibody labeled with horseradish peroxidase for 2 h of incubation at 4 °C, and the target bands' gray values were analyzed after development.

2.14. Detection of inflammatory responses and oxidative damage in CC

RT-qPCR was carried out to quantify oxidative damage markers (SOD and GSH-Px) and inflammatory factors (IL-6, IL-8 and TNF-α). After Trizol extraction, 10 μg of the total RNA from the cells to be tested was reverse transcribed into cDNA and then amplified (reaction conditions: 40 cycles of 95 °C for 30s, 95 °C for 10s, and 60 °C for 30s). Invitrogen (USA) was commissioned to design and construct the primer sequences (Table 1). $2^{-\triangle\triangle CT}$ calculated gene expression relative to GAPDH.

2.15. CYP3A4 and CYP2C8 expression detection

WB and RT-qPCR measured CYP3A4 and CYP2C8 expression in three groups of cells, and in HeLa, SiHa and End1/E6E7, so as to confirm the correlation of CYP3A4 and CYP2C8 with CC.

2.16. Tumorigenesis in nude mice

Forty mice were randomly divided into 2 groups (20 mice in each group), HeLa and SiHa were injected into the subcutaneous tissue of the axilla of mice (0.2mL/mouse) at the concentration of 1×10^7/mL, respectively, and fed for 7 days until the presence of tumor nodules at the injection site that was considered successful modeling. The successfully modeled mice were then randomly divided into 2 groups, one group was injected with 10 mg/kg of Nano-HSA-PTX and the other group was injected with the same amount of normal saline for 3 d. Mice injected with Nano-HSA-PTX were used as Nano-HSA-PTX group ($n = 10$), and those injected with normal saline were used as control group ($n = 10$). The culture was continued for 15 days, and 3 mice in each group were randomly selected at 5 d intervals and sacrificed by cervical dislocation under anesthesia. The intact subcutaneous tumor tissues were separated, weighed, and the volume was calculated.

2.17. Hematoxylin-eosin (HE) staining

The above tumor tissues were formaldehyde-fixed, paraffin-embedded, and sliced with a thickness of 4 μm. Xylene was de-waxed and gradient ethanol was fully hydrated for hematoxylin staining, differentiation and anti-blue. After completion, the sections were rinsed with double distilled water, stained with eosin and dehydrated using gradient ethanol for 2 min. Xylene was soaked 2 times and then fully air dried and the sections were sealed using neutral gum, the structural changes of tumor tissue (200 ×) were microscopically observed.

2.18. Statistics and methods

SPSS23.0 software was used for statistical analysis. All experiments in this study were repeated three times, and the results were expressed in the form of ($\bar{\chi} \pm s$). Independent samples *t*-test was used for comparison between groups, and variance analysis and Bonferroni test were used for comparison among groups. Statistical significance was indicated by $P < 0.05$.

Table 1
Primer sequences.

Gene	F (5′-3′)	R (5′-3′)
SOD	CACAACTGGTTCACCGCTTG	GCCCAACCAGACAGAGAATGA
GSH-Px	CGTGCAATCAGTTCGGACC	CCAGGCATCTCCCTTCCATTC
IL-6	GATGTTGCTGCTTCACTTC	CCTTGTTGGCTTATGTTCTG
IL-8	GGGCTGCATCTAAAGTAAATGG	CAGAACACTGCTGTAGAAGGTA
TNF-α	CTCTTCTCATTCCTGCTTG	CTCCACTTGGTGGTTTGCT
β-actin	CTAAGGCCAACCGTGAAAAG	ACCAGAGGCATACAGGGACA

3. Results

3.1. Characterization and observation of nano-HSA-PTX

As shown in Fig. 1A, Nano-HSA-PTX presents a relatively complete and uniform circular or quasi-circular shape under TEM, with scattered arrangement, large gaps, and relatively uniform particle size distribution, these results confirm that Nano-HSA-PTX has a typical nanoparticle characterisation. In addition, the particle size distribution and ZP of Nano-HSA-PTX cultured in 10%FBS-containing DMEM complete medium were not obviously different from those incubated in PBS with pH 7.4 ($P > 0.05$, Fig. 1B–D), indicating high stability of Nano-HSA-PTX in vivo.

3.2. Differences between nano-HSA-PTX and PTX

The EE% and DL% of Nano-HSA-PTX were (50.03 ± 2.93)% and (9.50 ± 0.95)%, respectively, which were significantly increased compared with PTX ($P < 0.05$, Fig. 2A and B). By comparing the drug release rate between the two, it can be seen that normal PTX was completely released within 6 h; however, the release rate of Nano-HSA-PTX decreased obviously, and the metabolism was complete at about 22 h (Fig. 2C). It can be seen that compared with PTX, Nano-HSA-PTX has higher drug loading efficiency and more stable drug release efficiency.

3.3. Cytotoxicity observation

As indicated by MTT assay results, under the treatment of Nano-HSA-PTX, the activity of HeLa and SiHa cells gradually decreased with the increase of the concentration (25, 50, 100, and 200 μg/mL) ($P < 0.05$); 200 μg/mL was selected as the dosage for subsequent research as cell viability was the lowest under this concentration (HeLa: 0.13 ± 0.01, SiHa: 0.14 ± 0.03) ($P < 0.05$, Fig. 3A and B).

3.4. Influences of Nano-HSA-PTX on CC cell proliferation, invasion and migration

The cell growth of Nano-HSA-PTX and PTX groups were markedly lower compared with the control group, and the cell absorbance was lower in Nano-HSA-PTX group versus PTX group ($P < 0.05$, Fig. 4A and B). Similarly, the cell cloning rate was determined to be the highest in the control group by the cell cloning experiment among the three groups, and that of the Nano-HSA-PTX group was even lower when compared to the PTX group ($P < 0.05$, Fig. 4C and D). The number of membrane-penetrating cells was the highest in the

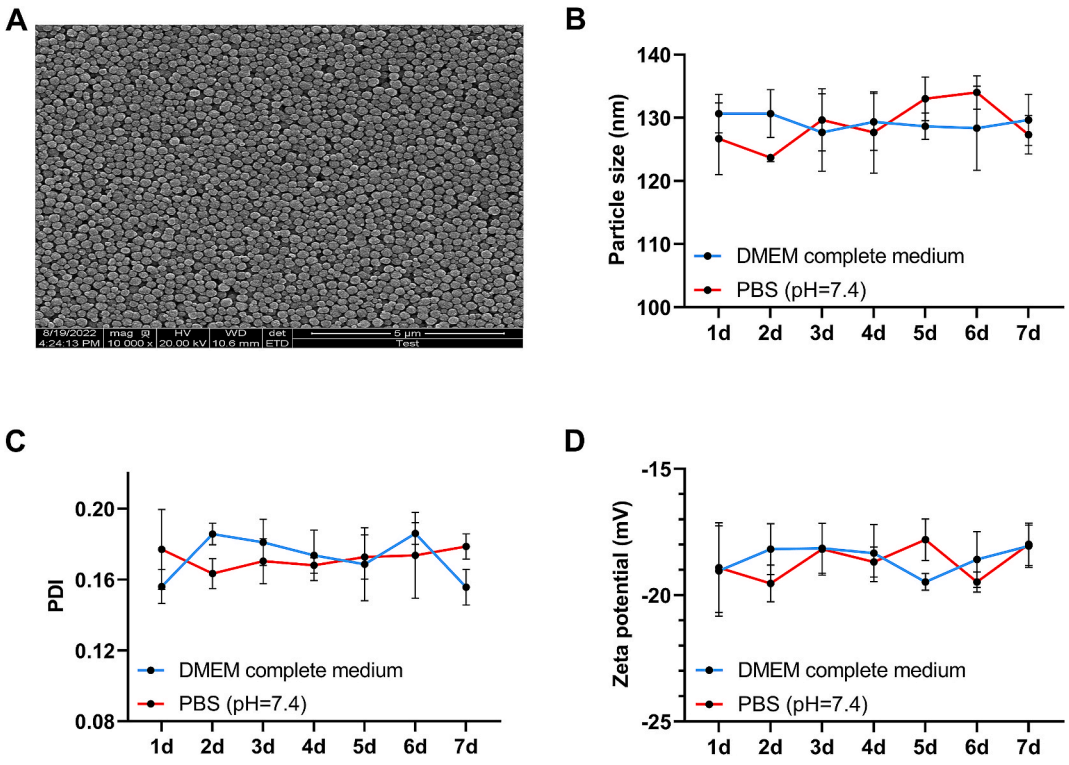

Fig. 1. Characterization and observation of Nano-HSA-PTX. (A) Morphological characteristics of Nano-HSA-PTX observed under TEM. (B) Particle size distribution of Nano-HSA-PTX. (C) PDI of Nano-HSA-PTX. (D) ZP of Nano-HSA-PTX.

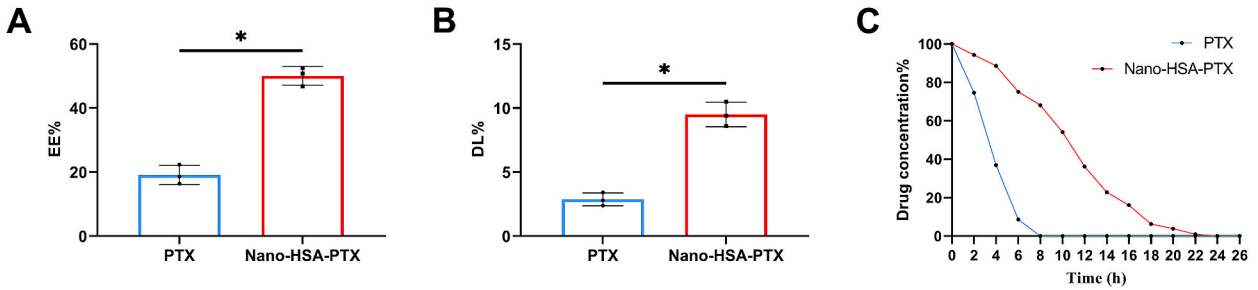

Fig. 2. Differences between Nano-HSA-PTX and PTX. (A) Comparison of EE% between Nano-HSA-PTX and PTX. (B) Comparison of DL% between Nano-HSA-PTX and PTX. (C) Comparison of drug release rate between Nano-HSA-PTX and PTX. *P < 0.05.

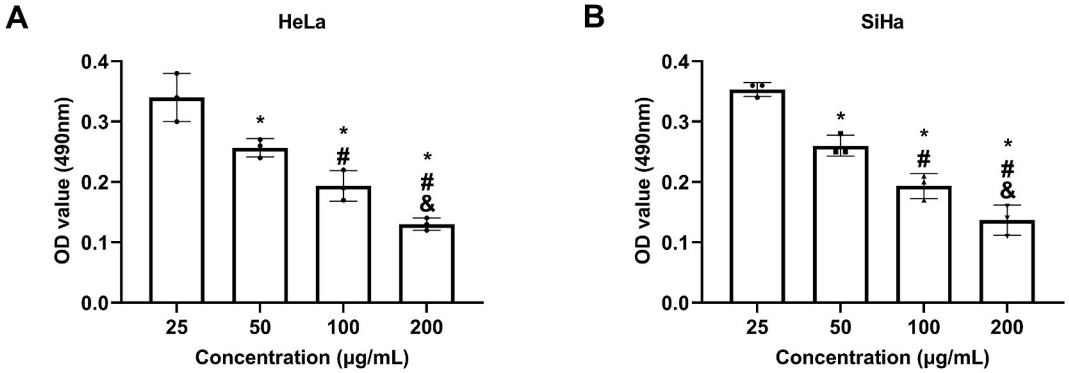

Fig. 3. Cytotoxicity observation. (A) Toxicity of Nano-HSA-PTX to HeLa. (B) Toxicity of Nano-HSA-PTX to SiHa. * means P < 0.05 compared with the concentration of 25 μg/mL; # means P < 0.05 compared with the concentration of 50 μg/mL; & means P < 0.05 compared with the concentration of 100 μg/mL.

control group and the lowest in the Nano-HSA-PTX group among the three groups (P < 0.05, Fig. 4E and F). And consistent results were found in cell scratch assay, that is, the control group had the highest cell migration rate and the Nano-HSA-PTX group had the lowest (P < 0.05, Fig. 4G and H). It can be seen that both PTX and Nano-HSA-PTX can inhibit the growth and malignant invasive ability of CC cells, and the inhibitory effect of Nano-HSA-PTX is more significant.

3.5. Impacts of Nano-HSA-PTX on CC cell apoptosis

The apoptosis rate of the control group was lower than that of the other two groups. The apoptosis rates of HeLa and SiHa in the Nano-HSA-PTX group were (12.66 ± 0.66)% and (13.55 ± 0.68)%, respectively, which were even higher compared with the PTX group (P < 0.05, Fig. 5A and B). According to apoptotic protein detection results, the control group had the lowest Bax protein and the highest Bcl-2 protein among the three groups, while the opposite was true in the Nano-HSA-PTX group, that is, Bax protein in the Nano-HSA-PTX group was the highest and Bcl-2 was the lowest in this group (P < 0.05, Fig. 5C–F). These results suggest that Nano-HSA-PTX can promote CC cell apoptosis more effectively than PTX.

3.6. Impacts of Nano-HSA-PTX on inflammation and oxidative damage in CC cells

The Nano-HSA-PTX and PTX groups showed lower IL-6, IL-8 and TNF-α mRNA levels and higher SOD and GSH-Px mRNA levels than the control group (P < 0.05); and more significant improvements of inflammatory factors and oxidative damage indicators were observed in the Nano-HSA-PTX group as compared to the PTX group (P < 0.05, Fig. 6A–D).

3.7. Impacts of Nano-HSA-PTX on CYP3A4 and CYP2C8

The Nano-HSA-PTX and PTX groups showed lower CYP3A4 and CYP2C8 levels than the control group; and compared with the PTX group, CYP3A4 and CYP2C8 were lower in the Nano-HSA-PTX group (P < 0.05, Fig. 7A and B). Further detection of CYP3A4 and CYP2C8 expression in HeLa, SiHa and End1/E6E7 showed higher CYP3A4 and CYP2C8 in HeLa and SiHa than in End1/E6E7 (P < 0.05, Fig. 7C). That is, Nano-HSA-PTX and PTX inhibited the expression of CYP3A4 and CYP2C8 in CC cells.

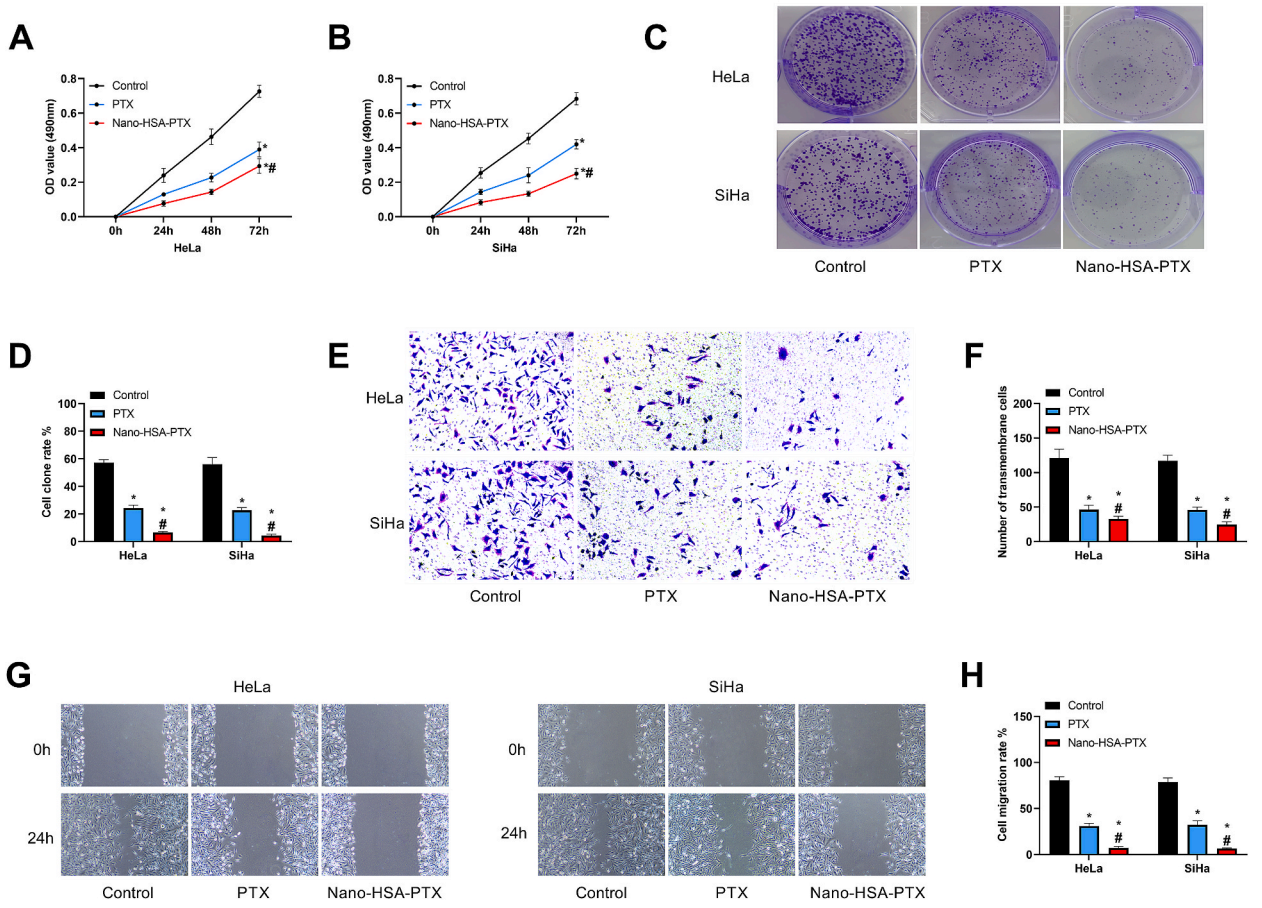

Fig. 4. Influences of Nano-HSA-PTX on CC cell proliferation, invasion and migration. (A) Cell growth curve of HeLa. (B) Cell growth curve of SiHa. (C) Cell cloning assay results. (D) Cell cloning rates of HeLa and SiHa. (E) Transwell assay results (200 ×). (F) The number of transmembrane cells of HeLa and SiHa. (G) Cell scratch assay results. (H) Cell migration rates of HeLa and SiHa. * means $P < 0.05$ compared with the control group; # means $P < 0.05$ compared with the PTX group.

3.8. Impacts of Nano-HSA-PTX on living tumor

At day 5–15, the tumor volume and weight in the control group were significantly higher than those in the Nano-HSA-PTX group ($P < 0.05$, Fig. 8A–D). HE staining results of tumor tissues showed that tumor cells in the control group transplanted with HeLa and SiHa grew in clusters and swirls; the cells were oval or round, with large nuclei and pathological mitoses; the nuclei were stained deeply, and necrosis lesions were seen among the nuclei that were pyknosis, dissolution and fragmentation, showing homogeneous red staining. In contrast, the tumor tissues in the Nano-HSA-PTX group showed abundant blood supply, well-defined boundaries, fish-cut like profile, relatively uniform tumor cell size, and light color (Fig. 8D).

4. Discussion

PTX, as a very common drug in CC chemotherapy, is widely used in clinical practice [16]. With the widespread application of PTX, its toxicity and drug resistance have become the key issues that affect its efficacy [13]. How to improve the effect of PTX while reducing its toxicity is the current research hotspot and difficulty. Drug-loaded NPs are one of the important research achievements in modern high-tech fields, which are especially suitable for tumor chemotherapy drugs with high drug resistance and toxicity [14,15]. In previous research, we have found significantly improved efficacy of chemotherapy drugs such as oxaliplatin in the form of drug-loaded nano-particles [16]. However, there is still a lack of research on PTX NPs and CC. Therefore, this study is of great significance to follow-up related research and future treatment of CC by exploring the effect of Nano-HSA-PTX on CC.

First, it can be seen that under TEM, Nano-HSA-PTX has a stable internal structure, with obviously increased EE% and DL%. In addition, drug release testing showed that PTX was basically completely released in 6 h, while the release cycle of Nano-HSA-PTX could reach about 22 h, suggesting that Nano-HSA-PTX can make up for the shortcomings of fast metabolism and short half-life of PTX. In previous studies, we also found that drug delivery by NPs is highly effective in improving the utilization rate of doxorubicin,

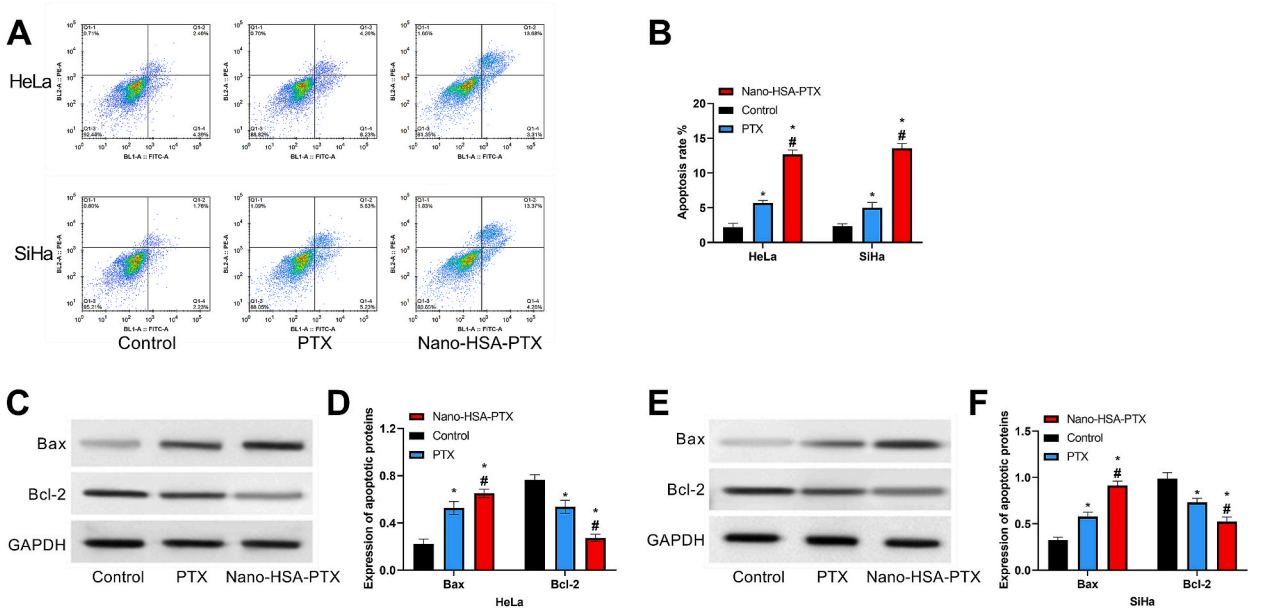

Fig. 5. Impacts of Nano-HSA-PTX on CC cell apoptosis. (A) Flow cytometry results. (B) Apoptosis rates of HeLa and SiHa. (C) Western blotting results of HeLa. (D) Bax and Bcl-2 protein expression in HeLa. (E) Western blotting results of SiHa. (F) Bax and Bcl-2 protein expression in SiHa. * means $P < 0.05$ compared with the control group; # means $P < 0.05$ compared with the PTX group.

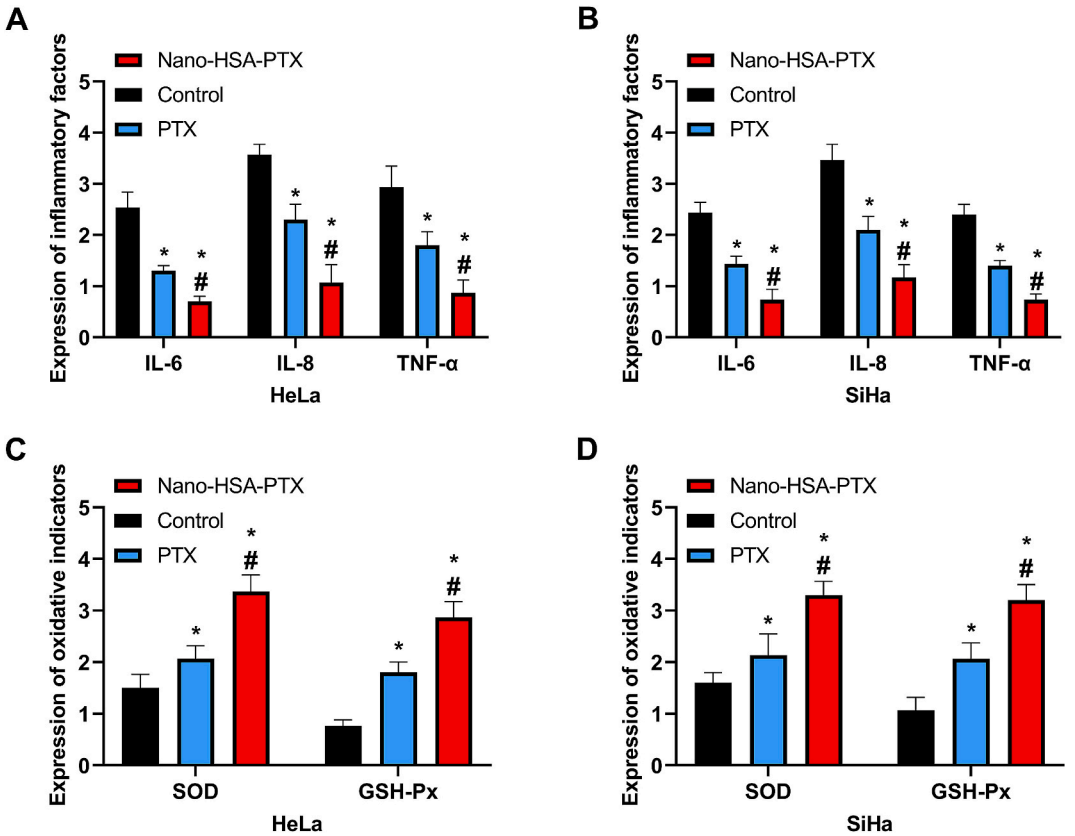

Fig. 6. Impacts of Nano-HSA-PTX on inflammation and oxidative damage in CC cells. (A) Expression of inflammatory factors in HeLa. (B) Expression of inflammatory factors in SiHa. (C) Expression of oxidative damage indexes in HeLa. (D) Expression of oxidative damage indexes in SiHa. * means $P < 0.05$ compared with the control group; # means $P < 0.05$ compared with the PTX group.

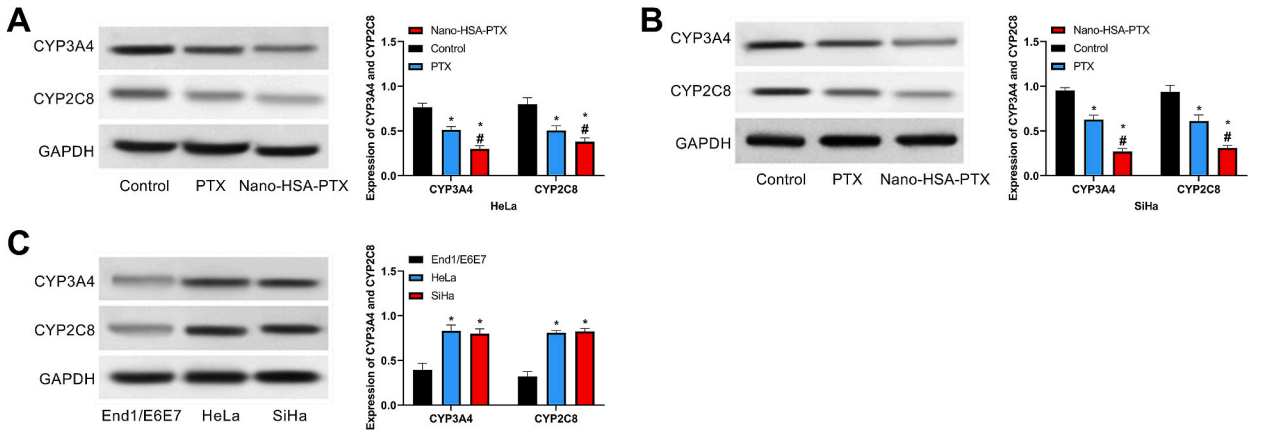

Fig. 7. Impacts of Nano-HSA-PTX on CYP3A4 and CYP2C8. (A) CYP3A4 and CYP2C8 protein expression in HeLa. (B) d and CYP2C8 protein expression in SiHa. (C) CYP3A4 and CYP2C8 protein expression in End1/E6E7, HeLa and SiHa. * means $P < 0.05$ compared with the control group; # means $P < 0.05$ compared with the PTX group.

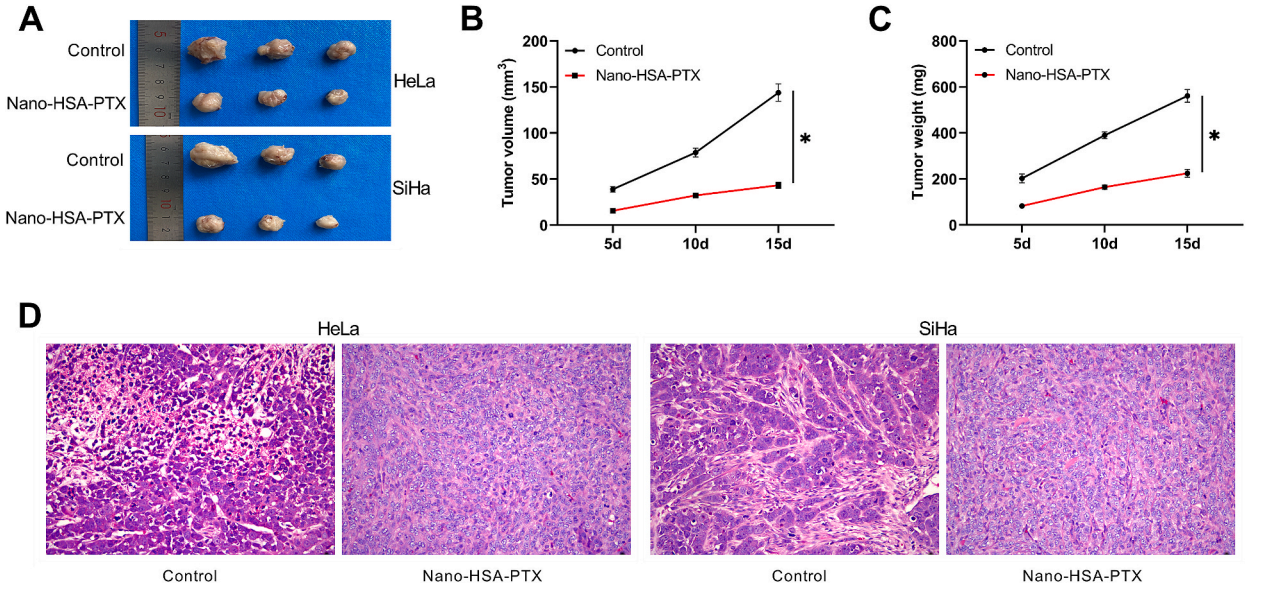

Fig. 8. Impacts of Nano-HSA-PTX on living tumor. (A) Tumor growth of transplanted HeLa and SiHa. (B) Changes in tumor volume. (C) Changes in tumor weight. (D) HE staining of tumor tissue (200 ×). *$P < 0.05$.

ceftizoxime and some other drugs [17,18], which also demonstrates the great application prospect of NPs in the clinical field in the future.

Then, we determined by cytotoxicity assay that the feasible dosage of Nano-HSA-PTX was 200 μg/mL. At this dose, Nano-HSA-PTX showed a better effect than PTX in inhibiting the activity, invasion and migration of CC cell lines HeLa and SiHa, while contributing to evidently higher apoptosis rate and Bax protein expression and lower Bcl protein expression in the Nano-HSA-PTX group compared with the PTX group. In addition, the Nano-HSA-PTX group exhibited obviously alleviated inflammatory reactions and oxidative damage in cells than the PTX group. It suggests that Nano-HSA-PTX can enhance the killing effect and safety of PTX on CC cells, thus improving the chemotherapy effect for CC. Similarly, Liu et al. showed that NP-loaded doxorubicin can further inhibit the proliferation of bladder cancer cells [19], which also corroborates our experimental results and highlights the important significance of NP-loaded drugs in tumor chemotherapy in the future. We believe that the improved effect of Nano-HSA-PTX on PTX may be due to the extremely small and dense molecular structure of NPs, which can quickly enter various tissues and cells of the human body and maximize the bioavailability of the loaded drugs; on the other hand, stable molecular packages can be formed to avoid premature volatilization due to the drug's own metabolic mechanism [20].

CYP3A4 and CYP2C8 have been considered as the oncogenes in situ of CC [21], with a close relationship with PTX [22]. We hypothesize that this may also be the influencing pathway of Nano-HSA-PTX on CC cells. For verification, we detected their expression

and found down-regulated CYP3A4 and CYP2C8 in PTX and Nano-HSA-PTX groups, as well as their increased levels in CC cell lines, which are consistent with previous experimental results [23,24] and can also preliminarily confirm our viewpoint. And given the role as oncogenic genes of CYP3A4 and CYP2C8 in CC, the inhibitory effects of PTX and Nano-HSA-PTX on them also reveal the potential molecular therapeutic approaches for CC. Of course, this requires further confirmation through more experiments.

Finally, through nude mouse tumorigenicity assay, Nano-HSA-PTX was found to exert excellent effects on the actual tumorigenesis of CC, with the pathological damage in tumor tissues significantly improved compared with the control group. It suggests that the future clinical application of Nano-HSA-PTX may optimize the current status of PTX in the treatment of CC, thus providing a more reliable security guarantee for the prognosis of patients.

However, there are still many issues to be confirmed before the clinical application of Nano-HSA-PTX, such as the dosage, time, and toxic and side effects of Nano-HSA-PTX in humans. Besides, how Nano-HSA-PTX influences CC cells through CYP3A4 and CYP2C8 needs further experimental confirmation. Finally, changes in CC cell proliferation, invasion and migration cycle under Nano-HSA-PTX intervention should be investigated to further understand the role of Nano-HSA-PTX in CC.

5. Conclusion

Nano-HSA-PTX can effectively enhance the killing effect of PTX on CC cells and alleviate oxidative damage, which may be related to the inhibition of CYP3A4 and CYP2C8 expression. In the future, Nano-HSA-PTX may effectively improve the therapeutic effect of PTX on CC and provide a more reliable guarantee for the improvement of patient outcomes.

Ethics approval and consent to participate

All procedures were conducted in accordance with the Animal Care guidelines and were approved by the Animal Ethics Committee of the Infectious Animal Laboratory, Jiangsu Institute of Schistosomiasis Control(approval No. 20190303-18).

Funding

This work is supported by the scientific research project plan of Wuxi Municipal Health Commission (NO.M202007); Wuxi Science and Technology Plan Project (NO·N2020X018); Top Talent Support Program for young and middle-aged people of Wuxi Health Committee; (NO.bj2020111;NO.hb2023115); National Nature Science Foundation of China (NO.81971335).

Data availability statement

The data in this article can be obtained from the corresponding author under reasonable circumstances.

Additional information

No additional information is available for this paper.

CRediT authorship contribution statement

Haojue Wang: Writing – review & editing, Writing – original draft. **Dajun Xiang:** Writing – review & editing, Writing – original draft. **Xianyi Lu:** Formal analysis, Data curation. **Ling Fang:** Methodology, Investigation. **Chengjun Cui:** Visualization, Validation. **Qifeng Shi:** Methodology, Investigation. **Xiaojun Yang:** Conceptualization.

Declaration of competing interest

The authors declare that the research was conducted in the absence of any commercial or financial relationships that could be construed as a potential conflict of interest.

References

[1] C.A. Johnson, D. James, A. Marzan, M. Armaos, Cervical cancer: an overview of pathophysiology and management, Semin. Oncol. Nurs. 35 (2019) 166–174, https://doi.org/10.1016/j.soncn.2019.02.003.

[2] S.L. Bedell, L.S. Goldstein, A.R. Goldstein, A.T. Goldstein, Cervical cancer screening: past, present, and future, Sex. Med. Rev. 8 (2020) 28–37, https://doi.org/10.1016/j.sxmr.2019.09.005.

[3] S.A. Pimple, G.A. Mishra, Global strategies for cervical cancer prevention and screening, Minerva Ginecol. 71 (2019) 313–320, https://doi.org/10.23736/s0026-4784.19.04397-1.

[4] S. Revathidevi, A.K. Murugan, H. Nakaoka, I. Inoue, A.K. Munirajan, APOBEC: a molecular driver in cervical cancer pathogenesis, Cancer Lett. 496 (2021) 104–116, https://doi.org/10.1016/j.canlet.2020.10.004.

[5] Y. Lin, Z. Shen, T. Tao, C. Xu, K. Xia, Q. Xuan, Study on the effect of polymer nano-loaded drug system on bladder cancer perfusion, J. Nanosci. Nanotechnol. 21 (2021) 955–961, https://doi.org/10.1166/jnn.2021.18638.

[6] R. Peng, D. Yang, X. Qiu, Y. Qin, M. Zhou, Preparation of self-dispersed lignin-based drug-loaded material and its application in avermectin nano-formulation, Int. J. Biol. Macromol. 151 (2020) 421–427, https://doi.org/10.1016/j.ijbiomac.2020.02.114.

[7] S. Peretz Damari, D. Shamrakov, M. Varenik, E. Koren, E. Nativ-Roth, Y. Barenholz, O. Regev, Practical aspects in size and morphology characterization of drug-loaded nano-liposomes, Int. J. Pharm. 547 (2018) 648–655, https://doi.org/10.1016/j.ijpharm.2018.06.037.
[8] M. Rajendran, G. Iraivan, B.L. Ghayathri, P. Mohan, K.R. Chandran, H.P. Nagaiah, R.C.A. Selvaraj, Antibiotic loaded nano rod bone cement for the treatment of osteomyelitis, Recent Pat. Nanotechnol. 15 (2021) 70–89, https://doi.org/10.2174/1872210514666200811103724.
[9] B. Li, Q. Li, J. Mo, H. Dai, Drug-loaded polymeric nanoparticles for cancer stem cell targeting, Front. Pharmacol. 8 (2017) 51, https://doi.org/10.3389/fphar.2017.00051.
[10] L.E. Minion, D.M. Chase, J.H. Farley, L.J. Willmott, B.J. Monk, Safety and efficacy of salvage nano-particle albumin bound paclitaxel in recurrent cervical cancer: a feasibility study, Gynecol. Oncol. Res. Pract. 3 (2016) 4, https://doi.org/10.1186/s40661-016-0025-6.
[11] S. Chen, Z. Song, R. Feng, Recent development of copolymeric nano-drug delivery system for paclitaxel, Anti Cancer Agents Med. Chem. 20 (2020) 2169–2189, https://doi.org/10.2174/1871520620666200719001038.
[12] V.M. Rosen, I. Guerra, M. McCormack, A. Nogueira-Rodrigues, A. Sasse, V.C. Munk, A. Shang, Systematic review and network meta-analysis of bevacizumab plus first-line topotecan-paclitaxel or cisplatin-paclitaxel versus non-bevacizumab-containing therapies in persistent, recurrent, or metastatic cervical cancer, Int. J. Gynecol. Cancer 27 (2017) 1237–1246, https://doi.org/10.1097/igc.0000000000001000.
[13] L. Della Corte, F. Barra, V. Foreste, P. Giampaolino, G. Evangelisti, S. Ferrero, G. Bifulco, Advances in paclitaxel combinations for treating cervical cancer, Expet Opin. Pharmacother. 21 (2020) 663–677, https://doi.org/10.1080/14656566.2020.1724284.
[14] C. Cheng, C. Li, X. Zhu, W. Han, J. Li, Y. Lv, Doxorubicin-loaded FeO-ZIF-8 nano-composites for hepatocellular carcinoma therapy, J. Biomater. Appl. 33 (2019) 1373–1381, https://doi.org/10.1177/0885328219836540.
[15] Y. Gao, J. Nai, Z. Yang, J. Zhang, S. Ma, Y. Zhao, H. Li, J. Li, Y. Yang, M. Yang, Y. Wang, W. Gong, F. Yu, C. Gao, Z. Li, X. Mei, A novel preparative method for nanoparticle albumin-bound paclitaxel with high drug loading and its evaluation both in vitro and in vivo, PloS one 16 (4) (2021) e0250670, https://doi.org/10.1371/journal.pone.0250670.
[16] J. Guo, Z. Yu, M. Das, L. Huang, Nano codelivery of oxaliplatin and folinic acid achieves synergistic chemo-immunotherapy with 5-fluorouracil for colorectal cancer and liver metastasis, ACS Nano 14 (2020) 5075–5089, https://doi.org/10.1021/acsnano.0c01676.
[17] C. Wang, X. Wei, G. Shao, Functional doxorubicin-loaded omega-3 unsaturated fatty acids nanoparticles in reversing hepatocellular carcinoma multidrug resistance, Med. Sci. Mon. Int. Med. J. Exp. Clin. Res. 27 (2021) e927727, https://doi.org/10.12659/msm.927727.
[18] M.S. Bacchu, M.R. Ali, M.A.A. Setu, S. Akter, M.Z.H. Khan, Ceftizoxime loaded ZnO/L-cysteine based an advanced nanocarrier drug for growth inhibition of Salmonella typhimurium, Sci. Rep. 11 (2021) 15565, https://doi.org/10.1038/s41598-021-95195-0.
[19] B. Liu, X. Gao, B. Han, G. Chen, S. Song, H. Bo, Mouse model to explore the therapeutic effect of nano-doxorubicin drug delivery system on bladder cancer, J. Nanosci. Nanotechnol. 21 (2021) 914–920, https://doi.org/10.1166/jnn.2021.18651.
[20] T.C. Wu, P.Y. Lee, C.L. Lai, C.H. Lai, Synthesis of multi-functional nano-vectors for target-specific drug delivery, Polymers 13 (2021), https://doi.org/10.3390/polym13030451.
[21] J.A. Agundez, Cytochrome P450 gene polymorphism and cancer, Curr. Drug Metabol. 5 (2004) 211–224, https://doi.org/10.2174/1389200043335621.
[22] T. Diab, S.S. Alkafaas, T.I. Shalaby, M. Hessien, Paclitaxel nanoparticles induce apoptosis and regulate TXR1, CYP3A4 and CYP2C8 in breast cancer and hepatoma cells, Anti Cancer Agents Med. Chem. 20 (2020) 1582–1591, https://doi.org/10.2174/1871520620666200504071530.
[23] J. Hofman, D. Vagiannis, S. Chen, L. Guo, Roles of CYP3A4, CYP3A5 and CYP2C8 drug-metabolizing enzymes in cellular cytostatic resistance, Chem. Biol. Interact. 340 (2021) 109448, https://doi.org/10.1016/j.cbi.2021.109448.
[24] L.A. Marcath, K.M. Kidwell, A.C. Robinson, K. Vangipuram, M.L. Burness, J.J. Griggs, C.V. Poznak, A.F. Schott, D.F. Hayes, N.L. Henry, D.L. Hertz, Patients carrying CYP2C8*3 have shorter systemic paclitaxel exposure, Pharmacogenomics 20 (2019) 95–104, https://doi.org/10.2217/pgs-2018-0162.